ACCSCIENCE PUBLISHING

Journal of Seismic Exploration

ARTICLE

Enhanced amplitude variation with incident angle inversion with Cauchy regularization using ensemble smoother-based data assimilation

Rui Liao and Ronghuo Dai*

Department of Statistics, School of Mathematical Sciences, China West Normal University, Nanchong, Sichuan, China

Abstract

Amplitude variation with incident angle (AVA) inversion for partial angle stack seismic data is an extension of acoustic impedance inversion. It adopts the P-wave reflection coefficient to link seismic amplitude information with elastic parameters and incident angle. This method generalizes conventional acoustic impedance inversion to pre-stack seismic data, enabling the effective inversion of multiple elastic parameters by utilizing seismic data acquired at different incident angles, such as angle gather data or partial angle stack data. This study addresses the limitations of commonly used AVA inversion with Cauchy regularization. Due to the non-linearity of Cauchy regularization, the iterative re-weighted least squares algorithm is extensively employed. It has been shown that the accuracy of inversion results of this non-linear inversion algorithm is highly dependent on the initial solution. When geological conditions are complex, the initial solution must be close to the optimal solution to ensure accurate inversion results. To address this challenge, this study proposes combining the ensemble smoother with multiple data assimilation (ES-MDA) and AVA inversion with Cauchy sparse regularization. Specifically, the posterior mean of ES-MDA is used as the initial solution for AVA inversion with Cauchy sparse regularization. ES-MDA is a stochastic method that solves inverse problems by iteratively updating an ensemble of model realizations, yielding a solution that closely approximates the optimal solution. Practical application indicates that, compared with AVA inversion with Cauchy sparse regularization using a standard initial solution, the proposed method achieves improved accuracy in estimated elastic parameters. The research findings offer new technical approaches for seismic prediction with AVA inversion in complex reservoirs.

Keywords: Seismic inversion; Ensemble smoother with multiple data assimilation; Elastic parameters; Amplitude variation with incident angle inversion; Cauchy regularization

***Corresponding author:**
Ronghuo Dai
(daironghuo@yeah.net)

Citation: Liao R, Dai R. Enhanced amplitude variation with incident angle inversion with Cauchy regularization using ensemble smoother-based data assimilation. *J Seismic Explor*. doi: 10.36922/JSE025500125

Received: December 10, 2025

Revised: January 10, 2026

Accepted: February 4, 2026

Published online: March 31, 2026

1. Introduction

Due to the advancements in global oil and gas exploration and development, exploration targets have gradually shifted from simple structural reservoirs to complex lithologic reservoirs, unconventional reservoirs, and deep-to-ultra-deep domains. Such reservoirs often exhibit pronounced heterogeneity and complex pore fluid properties, posing

significant challenges for predicting reservoir properties and identifying fluid types using traditional seismic amplitude data.

Elastic parameters that are sensitive to lithology and fluids, such as P-impedance, P-velocity, S-impedance, S-velocity, Lamé parameters, and density, can be directly estimated from seismic traces at different incidence angles using pre-stack inversion techniques. These techniques are fundamentally based on the Zoeppritz equation[1,2] and its approximations and have become a core method for accurately characterizing complex reservoirs. Among these, amplitude variation with incident angle (AVA) inversion serves as a bridge, tightly linking pre-stack data with well-log data. Its clear physical significance and relatively straightforward computation have led to widespread adoption in the industry. By combining AVA inversion from multiple angles to invert subsurface elastic parameters, the multi-solution nature of the inversion problem can be effectively reduced, enhancing the accuracy of reservoir characterization. The core of AVA inversion lies in estimating the subsurface elastic parameters. This methodology is based on the Zoeppritz equation,[2] which is complex and difficult to apply directly, giving rise to many approximate methods that simplify it from different perspectives. Aki and Richards[1] proposed linear approximations suitable for weakly heterogeneous media and small incident angles. Shuey[3] reconfigured the Aki–Richards equation using P-velocity, Poisson's ratio, and density; this version is widely used in gas reservoir characterization. Russell *et al.*[4] introduced the effect of pore fluid, directly estimating the fluid indicator factor. Xiao *et al.*[5] proposed a non-linear pre-stack AVA inversion method incorporating lithology constraints. Within a Bayesian framework, their method introduces correlations between elastic parameters to establish constraints, demonstrating enhanced resolution and stability. Bao *et al.*[6] developed an AVO inversion method by replacing approximate isotropic Zoeppritz equations with the exact isotropic Zoeppritz equations, improving the accuracy of the isotropic model. Ye *et al.*[7] analyzed errors in the Zoeppritz approximate equations using log data and demonstrated the feasibility of full-angle pre-stack density inversion through AVO modeling. As seismic exploration targets become increasingly complex and large-offset data are widely adopted, the industry's demand for AVA inversion methods applicable to strong heterogeneous media and wide incident angles has grown. To address this challenge, Zhou *et al.*[8] proposed the joint multi-wave inversion using the exact Zoeppritz equation with a modified Cauchy prior distribution. By establishing a stochastic model for reservoir reflectivity variation, Li[9] derived a reservoir-characteristics-constrained AVO equation that allows pre-stack inversion to recover fluid-sensitive parameters. Lehocki *et al.*[10] effectively improved the accuracy of density inversion using high-order approximation of the Zoeppritz equations. Sun *et al.*[11] developed a high-precision fluid factor using a frequency-varying AVO inversion based on the Russell equation to extract frequency dispersion attributes.

However, the ill-posed nature of AVA inversion remains a significant challenge. To obtain stable and geologically reasonable inversion results, regularization is required.[12] Among numerous choices, Cauchy regularization is widely used in seismic inversion.[13-15] Due to its non-linearity, the iterative re-weighted least squares (IRLS) algorithm is commonly employed.[16] The accuracy of IRLS inversion is highly dependent on the initial solution, making its selection critical in seismic inversion with Cauchy regularization. Common approaches for generating initial solutions include zero-ordinary-solution,[17] well-log interpolation,[18] and velocity analysis.[19] When geological conditions are simple and non-linearity is limited, these initial solutions produce satisfactory inversion results without significantly affecting subsequent reservoir predictions or fluid identification. However, in complex geological settings, such as lithologic pinch-out, channels, steeply inclined strata, hydrocarbon reservoirs, or reservoirs with abrupt lateral variations of elastic parameters, the quality of the inversion results can be severely compromised. In these cases, the initial solution must be close to the optimal solution to ensure accuracy.

To address this limitation of AVA inversion with Cauchy regularization, we propose combining the ensemble smoother with multiple data assimilation (ES-MDA) and AVA inversion using Cauchy sparse regularization. ES-MDA, developed by Emerick and Reynolds,[20] enhances the handling of non-linear problems through ensemble statistics and multiple iterations. As an ensemble-based Bayesian inversion algorithm, ES-MDA has been successfully applied in seismic inversion, effectively addressing the bottlenecks of traditional methods in handling non-linearity and quantifying uncertainty.[21] ES-MDA is a stochastic method that solves inverse problems by iteratively updating an ensemble of model realizations, producing a solution that approximates the optimal solution. However, seismic reservoir characterization often involves high-dimensional geophysical data. Consequently, the number of high-dimensional ensemble models for complete two-dimensional (2D) profiles or three-dimensional (3D) volumes can become prohibitively large, limiting the method's practical application.[22] In this study, we implement ES-MDA in a computationally feasible manner, applying it trace-by-trace to exploit its

ability to approximate the optimal solution. Research indicates that, when combined with ES-MDA, the proposed AVA inversion method achieves improved accuracy in estimating elastic parameters.

2. Methods

2.1. Amplitude variation with incident angle inversion with Cauchy regularization

The AVA inversion is a technique used to extract the elastic properties of subsurface rocks—such as velocity and density—from seismic data. Specifically, it analyzes how the amplitude of seismic reflections changes with angle, using pre-stack angle gathers or partially angle-stack data as the primary input. These properties encompass fundamental elastic parameters—such as P-wave velocity, S-wave velocity, and density—as well as derived attributes such as Poisson's ratio, Young's modulus, Lamé parameters, fluid factors, and other relevant attributes. By estimating these parameters, a more comprehensive understanding of the physical characteristics and structure of underground rocks can be achieved, which is crucial for oil and gas exploration and development.

Currently, AVA inversion typically involves first estimating the relative variation rates of elastic parameters from pre-stack seismic data. Subsequently, the final elastic parameters are derived through their relationships with these relative variation rates of elastic parameters. In this context, the objective function for AVA inversion is formulated based on the Aki–Richards approximation of the P-wave reflection coefficient, as shown in **Equation 1**:

$$R_{pp}(\theta) \approx a(\theta)R_{vp} + b(\theta,\gamma)R_{vs} + c(\theta,\gamma)R_{\rho} \tag{1}$$

where, $a(\theta) = \sec^2\theta$, $b(\theta,\gamma) = -8\gamma^2\sin^2\theta$, $c(\theta,\gamma) = (1-4\gamma^2\sin^2\theta)$, θ represents the incident angle, $R_{pp}(\theta)$ represents the P-wave reflection coefficient, γ is the ratio of S-velocity to P-velocity, and R_{V_P}, R_{V_S}, and R_{ρ} are the relative variation rates of V_p, V_s, and ρ, respectively. Here, V_p, V_s, and ρ represent P-velocity, S-velocity, and density, respectively.

Using the seismic convolution model together with the approximate expression given in **Equation 1**, the forward equation for AVA inversion can be written as **Equation 2**:[23]

$$\mathbf{d} = \mathbf{Am} + \mathbf{n} \tag{2}$$

where **A** represents the forward operator incorporating the wavelet convolution operator and the approximate expression, $\mathbf{m} = [R_{Vp}, R_{Vs}, R_{\rho}]^T$ denotes the model parameters for AVA inversion, **d** represents the observations (i.e., the input seismic data), and **n** denotes the noise.

Typically, the AVA inversion is performed by minimizing a least squares objective function, regularized by a combination of Cauchy regularization and a priori model constraints to enhance both resolution and stability, as shown in **Equation 3**:

$$\min f(\mathbf{m}) = \| \mathbf{Am} - \mathbf{d} \|_2^2 + \lambda \text{Cauchy}(\mathbf{m}) + \alpha \| \mathbf{m} - \mathbf{m}_{prior} \|_2^2 \tag{3}$$

where m_{prior} represents the a priori model, as shown in **Equation 4**:

$$\text{Cauchy}(\mathbf{m}) = \sum_i \ln[1 + \frac{m^2(i)}{\sigma^2}] \tag{4}$$

where the parameters in the objective function are defined as follows: σ is the deviation parameter of the model m under the Cauchy criterion;[9] λ and α are the regularization parameters corresponding to the Cauchy and a priori model terms, respectively; and $m(i)$ denotes the i-th element of m.

The estimation of the final elastic parameters is typically a two-step process. First, the AVA inversion objective function is solved to obtain the relative variations of the elastic parameters. Second, these relative variations are integrated using established formulas to recover the absolute elastic properties.[15,24] Alternatively, other approximate expressions can be used to directly estimate elastic parameters through AVA inversion, such as Fatti's approximation,[25] Li and Zhang's approximation,[23] and related approaches.

2.2. Iteratively reweighted least squares algorithm

In general, the objective function in **Equation 3** is solved using the IRLS algorithm.[16] The basic steps of the IRLS method are as follows. From **Equation 4**, the derivative of the Cauchy regularization term (i.e., the second term in **Equation 3**) can be expressed as **Equation 5**:

$$\nabla \sum_{i=1}^{m} \frac{2m(i)}{m^2(i) + \sigma^2} = 2\mathbf{Q}(\mathbf{m})\mathbf{m} \tag{5}$$

where Q(m) is a diagonal matrix whose elements are $\frac{1}{\sigma^2 + m^2(i)}$.

Hence, the solution to **Equation 3** can be written as **Equation 6**:

$$\mathbf{A}^T\mathbf{Am} + \lambda\mathbf{Q}(\mathbf{m})\mathbf{m} + \alpha\mathbf{m} = \mathbf{A}^T\mathbf{d} + \alpha\mathbf{m}_{prior} \tag{6}$$

The basic idea of IRLS is as follows: Q(m) is treated as a weight matrix. To solve **Equation 3**, IRLS iteratively performs the following damped least-squares problem,

starting from a suitable initial solution, as shown in **Equation 7**:

$$\mathbf{m}^k = (\mathbf{A}^T\mathbf{A} + \lambda\mathbf{Q}(\mathbf{m}^{k-1}) + \alpha\mathbf{I})^{-1}(\mathbf{A}^T\mathbf{d} + \alpha\mathbf{m}_{prior}) \quad (7)$$

In each iteration, Q(m) is updated using the solution from the previous iteration. The solution of **Equation 7** can be obtained using commonly adopted methods, such as the conjugate gradient algorithm. The combined effect of the Cauchy regularization term and the inherent non-linearity of the forward equation makes the IRLS algorithm prone to convergence toward a local optimum during the inversion process. Consequently, the choice of the initial solution is a critical factor in AVA inversion. Despite this limitation, the iterative framework of IRLS is simple, robust, and widely used in the industry. In this study, quality control was employed to determine the regularization parameters, which required available well-log data. During quality control, the actual well logs were regarded as the answer for the inversion of near-well seismic traces, as they represent the actual geological characteristics of underground formations. The optimal regularization parameters were determined by performing quality control at well locations, including adjusting the value of the regularization parameter set, obtaining the inversion result from the near-well seismic traces for each regularization parameter set, and selecting the set that produces the best match with the corresponding well logs. The selected regularization parameters were then applied to the inversion for other seismic traces.

2.3. Ensemble smoother data assimilation

To construct a reliable initial solution, ES-MDA was integrated into the AVA inversion framework. ES-MDA approximates the posterior probability distribution through ensemble statistics. The core idea of ES-MDA is to iteratively and gradually incorporate observational information into an initial set of model parameters (i.e., multiple possible models). This process ensures that the updated parameter set not only better fits the observations but also reasonably reflects parameter uncertainties. The specific steps of the ES-MDA algorithm are as follows:[22]

(i) Define the ensemble size *n*, determine the number of data assimilation iterations *K*, and the inflation coefficient $\{\alpha_i, i = 1,2,...,K\}$ for each iteration.

(ii) Samples are drawn from the prior distribution of the model parameters to form the initial sample set $\{\mathbf{m}_j, j = 1,\ldots,n\}$. Let i=1.

(iii) Start the iteration. Simulate *n* zero-mean Gaussian random vectors $\{\mathbf{z}_j, j = 1,\ldots,n\}$, where $\mathbf{z}_j \sim N(0,\delta^2\mathbf{I})$, is the variance and $\mathbf{I}$ is the identity matrix. Then, the simulated random vectors are added to the measured seismic data as the perturbations, as shown in **Equation 8**:

$$\tilde{\mathbf{d}}_j = \mathbf{d} + \sqrt{\alpha_i}\mathbf{£}^{\frac{1}{2}}\mathbf{z}_j, j = 1,\ldots,n \quad (8)$$

where, **Ó** is the covariance matrix of the original data d, $\tilde{\mathbf{d}}_j$ is the *j*-th perturbed data vector.

(iv) Apply the forward operator A to each model parameter m_j in $\{\mathbf{m}_j, j = 1,\ldots,n\}$ to calculate the predictive data $\{\mathbf{d}_j, j = 1,\ldots,n\}$.

(v) Update the model parameters. For each model parameter, update $\mathbf{m}_j$ in the ensemble model $\{\mathbf{m}_j, j = 1,\ldots,n\}$,

$$\tilde{\mathbf{m}}_j = \mathbf{m}_j + \mathbf{£}_{m,d}(\mathbf{£}_{d,d} + \alpha_i\mathbf{£})^{-1}(\tilde{\mathbf{d}}_j - \mathbf{d}_j) \quad (9)$$

where, $\tilde{\mathbf{m}}_j$ is the *j*-th model after updating, $\mathbf{Ó}_{m,d}$ is the covariance matrix between the ensemble models and predictive data, and $\mathbf{Ó}_{d,d}$ is the covariance matrix of predictive data, as shown in **Equations 10** and **11**:

$$\mathbf{£}_{m,d} = \frac{1}{n-1}\sum_{j=1}^{n}(\mathbf{m}_j - \overline{\mathbf{m}})(\mathbf{d}_j - \overline{\mathbf{d}})^T \quad (10)$$

$$\mathbf{£}_{d,d} = \frac{1}{n-1}\sum_{j=1}^{n}(\mathbf{d}_j - \overline{\mathbf{d}})(\mathbf{d}_j - \overline{\mathbf{d}})^T \quad (11)$$

and, $(\Sigma_{d,d} + \alpha_i\Sigma)^{-1}$ is the so-called Kalman gain matrix. Here, $\overline{\mathbf{d}}$ and $\overline{\mathbf{m}}$ are the mean vectors of $\{\mathbf{d}_j, j = 1,\ldots,n\}$ and $\{\mathbf{m}_j, j = 1,\ldots,n\}$.

(vi) Replace the initial ensemble model $\{\mathbf{m}_j, j = 1,\ldots,n\}$ with the updated model $\{\tilde{\mathbf{m}}_j, j = 1,\ldots,n\}$.

(vii) Let i=i+1 and repeat steps (iii)–(vi) until the *K*-th iteration is completed, resulting in the final set of parameter samples $\{\mathbf{m}_j, j = 1,\ldots,n\}$ and derive the estimations of the posterior distribution of the model parameters.

In ES-MDA, the quality of results depends on the number of assimilation iterations n_α, the inflation coefficient α_i, and the Gaussian perturbations variance δ^2. Traditional ES-MDA approaches usually determine these parameters based on experience selection. Following the quality control strategy described earlier, we applied the same approach here to obtain optimal values for these parameters in ES-MDA.

Ensemble smoother with multiple data assimilation refines each ensemble model by minimizing the mismatch between observed data and model predictions, resulting in a series of model realizations that align with the observed outcomes. This method provides a stochastic solution to

an inverse problem by sequentially updating an ensemble of model variables through simultaneous assimilation of measurement data. Its solution is a good approximation of the optimal solution. Therefore, the posterior mean of the ES-MDA results was adopted as the initial solution of AVA inversion with Cauchy regularization.

However, seismic reservoir characterization often involves geophysical data of very high dimensionality. Consequently, the number of high-dimensional ensemble models for the whole 2D profiles or 3D volumes becomes prohibitively large, making direct application to real datasets infeasible.[22] Therefore, in this study, ES-MDA was not applied to the entire seismic dataset but was instead implemented in a computationally feasible manner on a trace-by-trace basis to take advantage of its ability to approximate the optimal solution.

3. Results

3.1. Numerical model tests

First, a 2D layered model that included multiple complex geological features, such as geological lens bodies, faults, and pinch-outs, was used to conduct numerical tests of the proposed method. The model is shown in Figure 1, where Figure 1A–C correspond to V_p, V_s, and ρ, respectively. Based on Aki–Richards' approximation, the corresponding P-wave reflection coefficients were computed for four distinct incident angles: 5°, 15°, 25°, and 35°. The corresponding synthetic seismic data were generated by convolving the reflection coefficients with a 25 Hz Ricker wavelet for each incident angle. Subsequently, the synthetic seismic data were corrupted by 15% zero-mean Gaussian random noise. The contaminated data are presented in Figure 2, where Figure 2A–D correspond to incident angles of 5°, 15°, 25°, and 35°, respectively.

To simulate the incompleteness of prior information in practical applications, the true model was subjected strong smoothing process, retaining only the fundamental low-frequency background trend while completely removing the high-frequency details such as reservoirs. The smooth models are shown in Figure 3, where Figure 3A–C correspond to V_p, V_s, and ρ, respectively. These models were used as the a priori model.

An ensemble smoother with multiple data assimilation was then applied to the noise-contaminated seismic data. For ES-MDA, the key parameters were set as follows: the number of integrated members was 1,000, the number of inner assimilation times was 4, and the perturbation parameter for the data was 0.0001. Due to the prohibitive computational cost of applying ES-MDA to the entire 2D model, the analysis was performed on a trace-by-trace basis instead. This approach is computationally feasible and takes advantage of the ability of ES-MDA to provide a good approximation of the optimal solution. The results of ES-MDA are shown in Figure 4. It can be observed that the lateral continuity is very poor, which is expected because ES-MDA was performed trace-by-trace without lateral constraints. However, the detailed features of the model were well estimated. Therefore, the ES-MDA results still represent a good approximation of the true model.

Next, the results from ES-MDA were used as the initial solution for the AVA inversion incorporating Cauchy regularization. The corresponding inversion results are shown in Figure 5. As a baseline for comparison, traditional AVA inversion was directly applied to the noise-contaminated data using the smooth model as the initial solution. The inversion results are shown in Figure 6. Both inversion results showed good agreement with the true model. However, the inversion results in Figure 5 exhibited more detailed features, as highlighted by the black rectangular boxes. Enlarged views of these regions are shown in Figures 7 and 8. As shown in Figure 7, the lateral continuity within the lens improved, and the pinch-out locations of the lens were clearer.

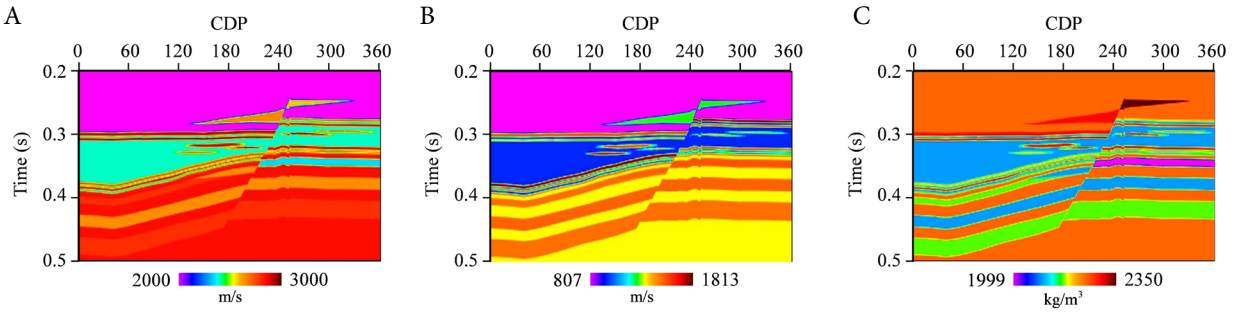

Figure 1. True model. (A) V_p. (B) V_s. (C) ρ.
Abbreviations: CDP: Common depth point; ρ: Density; V_p: P-wave velocity; V_s: S-wave velocity.

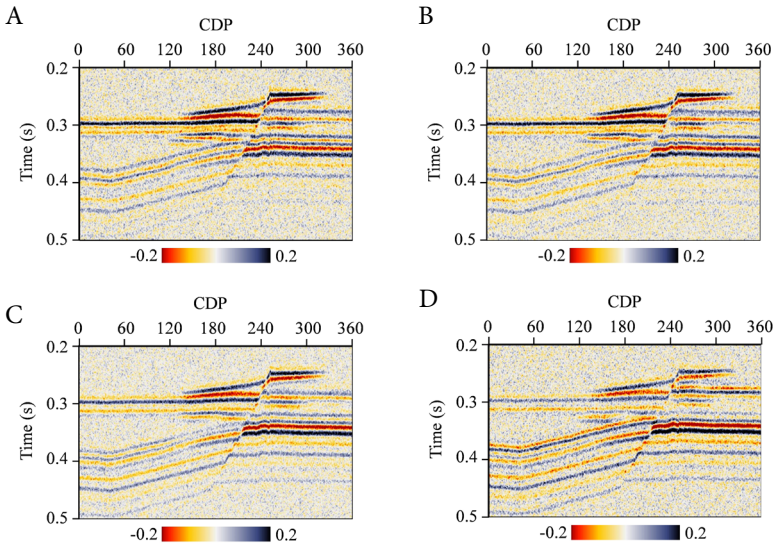

Figure 2. The noise-contaminated seismic data with different angles. (A) 5°, (B) 15°, (C) 25°, and (D) 35°.
Abbreviation: CDP: Common depth point.

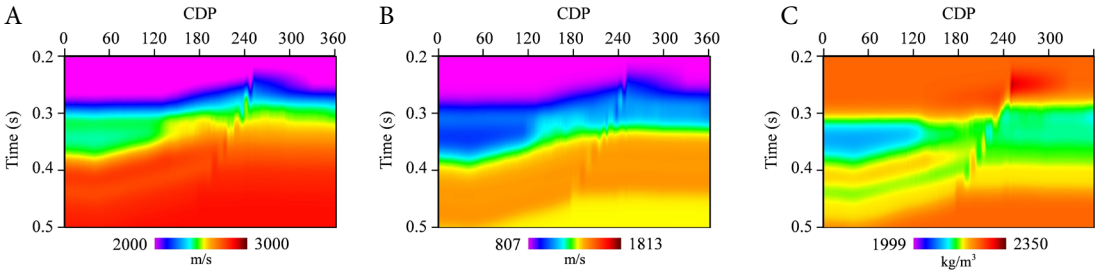

Figure 3. Smooth model. (A) V_p. (B) V_s. (C) ρ.
Abbreviations: CDP: Common depth point; ρ: Density; V_p: P-wave velocity; V_s: S-wave velocity.

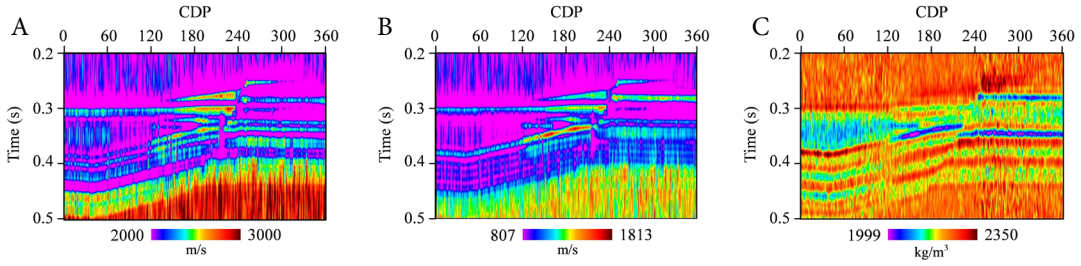

Figure 4. The results of ES-MDA. (A) V_p. (B) V_s. (C) ρ.
Abbreviations: CDP: Common depth point; ES-MDA: Ensemble smoother with multiple data assimilation; ρ: Density; V_p: P-wave velocity; V_s: S-wave velocity.

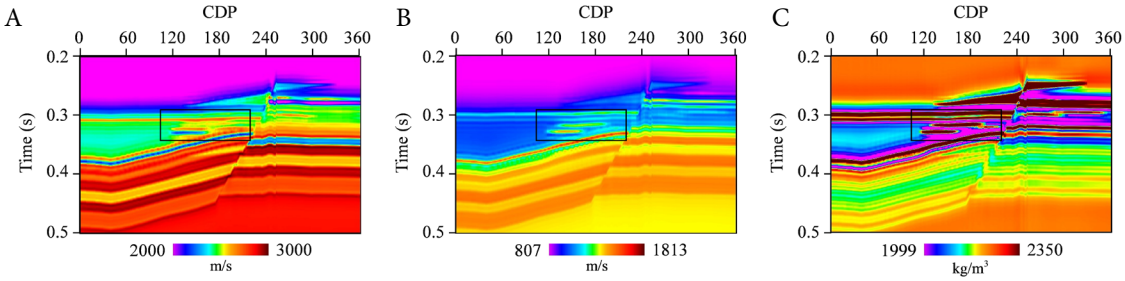

Figure 5. The inversion results of AVA inversion with Figure 4 as the initial solution. (A) V_p. (B) V_s. (C) ρ.
Abbreviations: AVA: Amplitude variation with incident angle inversion; CDP: Common depth point; ρ: Density; V_p: P-wave velocity; V_s: S-wave velocity.

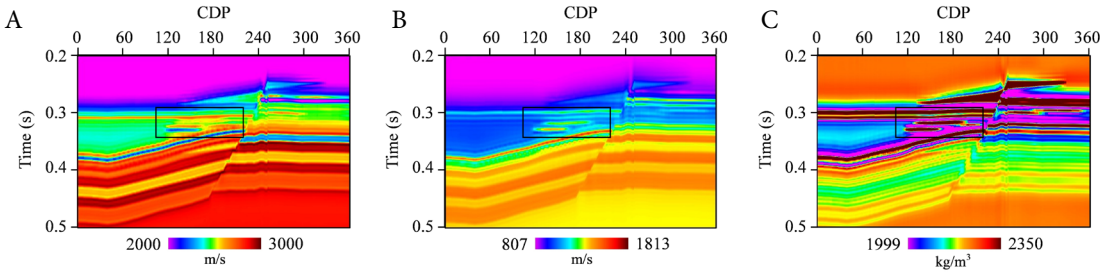

Figure 6. The inversion results of AVA inversion with Figure 3 as the initial solution. (A) V_p. (B) V_s. (C) ρ.
Abbreviations: CDP: Common depth point; ρ: Density; V_p: P-wave velocity; V_s: S-wave velocity.

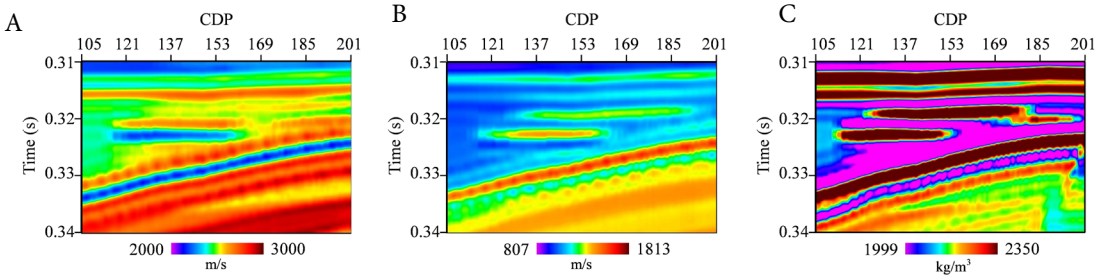

Figure 7. The enlarged views of the black rectangular box in Figure 5. (A) V_p. (B) V_s. (C) ρ.
Abbreviations: CDP: Common depth point; ρ: Density; V_p: P-wave velocity; V_s: S-wave velocity.

Due to the relatively small differences observed in the numerical model tests between the two methods, the root mean square error (RMSE) between the inversion results and the true model was calculated for both approaches (Table 1). It can be seen that the RMSE values obtained using ES-MDA as the initial solution are smaller than those obtained using the smooth model as the initial solution.

To illustrate the stability of the inversion in the numerical model tests, the variances of the inversion results were calculated, and corresponding variance maps were obtained. Figure 9 shows the variances of the inversion result. It can be observed that, in the numerical model tests, the variance of ρ is generally larger than that of V_p and V_s, which further confirms the well-known instability of density estimation in AVA inversion. During the quality control process, a small rectangular region within the black rectangular box in Figure 5 was used to select the optimal values of ES-MDA and regularization parameters. Consequently, for V_p and V_s, the variances in the middle-layer region were relatively smaller. Overall, the inversion stability was considered acceptable.

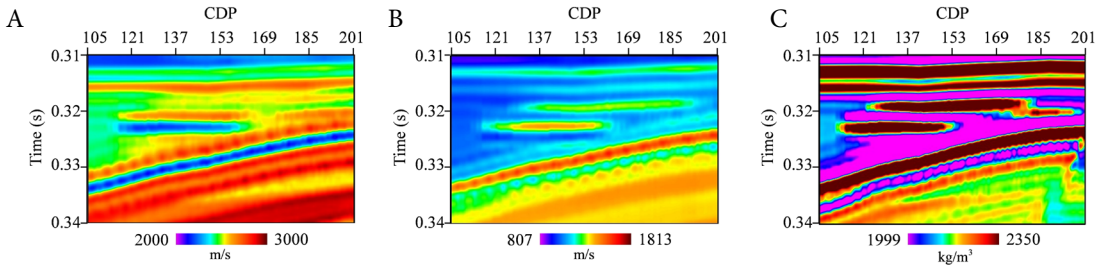

Figure 8. The enlarged views of the black rectangular box in Figure 6. (A) V_p. (B) V_s. (C) ρ.
Abbreviations: CDP: Common depth point; ρ: Density; V_p: P-wave velocity; V_s: S-wave velocity.

Table 1. The root mean square error between the two methods and the true model in the numerical model tests

Parameters	Methods	RMSE
P-wave velocity	AVA with a smooth model as the initial solution	0.0513
	AVA with ES-MDA as the initial solution	0.0500
S-wave velocity	AVA with a smooth model as the initial solution	0.0784
	AVA with ES-MDA as the initial solution	0.0721
Density	AVA with a smooth model as the initial solution	0.0553
	AVA with ES-MDA as the initial solution	0.0500

Abbreviations: AVA: Amplitude variation with incident angle inversion; CDP: Common depth point; ES-MDA: Ensemble smoother with multiple data assimilation; RMSE: Root mean square error.

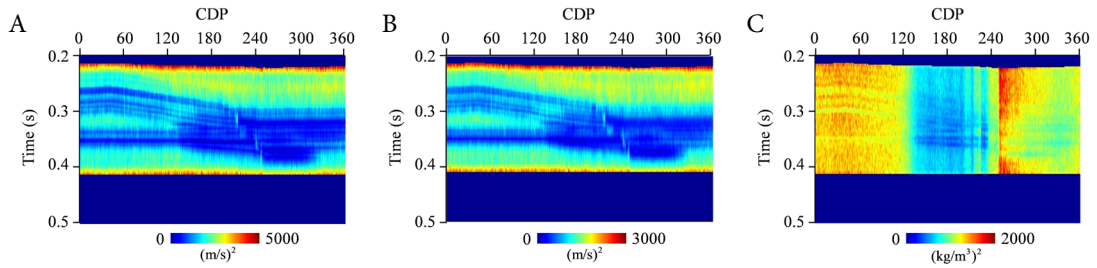

Figure 9. The variances of the inversion result. (A) V_p. (B) V_s. (C) ρ.
Abbreviations: CDP: Common depth point; ρ: Density; V_p: P-wave velocity; V_s: S-wave velocity.

3.2. Real data applications

To verify the effectiveness of AVA inversion using ES-MDA results as the initial solution, the proposed method was evaluated on a real seismic line acquired from a work area in East China (exact location withheld at the data owner's request). The dataset consisted of four partial-angle stacks with angle ranges of 2–12°, 12–22°, 22–32°, and 32–42°, respectively. These sections are shown in Figure 10. Three low-frequency trend models of V_p, V_s, and ρ were constructed based on well-log data and interpreted geological horizons. The dominant frequency of the seismic data is 22 Hz. Accordingly, a 22 Hz wavelet, extracted from well-log data and near-well seismic traces, was used for forward modeling in the ES-MDA process. For the ES-MDA, the key parameters were set as follows: the number of random simulations was 100, the number of inner assimilation times was 4, and the random perturbation parameter for seismic data was 0.1. The resulting ES-MDA outputs are shown in Figure 11. It can be observed that the ES-MDA results exhibited poor lateral continuity, but many detailed features were successfully reconstructed, which is critical for improving the subsequent AVA inversion results. The ES-MDA results were then used as the initial solution for AVA inversion with Cauchy regularization. For comparison, the AVA

inversion using the low-frequency trend models as the initial solution was also applied to the real seismic data. The inverted V_p, V_s, and ρ obtained using the two different methods are shown in Figures 12–14, respectively. In the inverted elastic parameters profiles, the actual impedance log intersecting this seismic line was also overlaid.

From the comparison, it can be seen that the geologic structures in the inversion results from both methods are consistent with the real seismic data profiles. All inverted elastic parameter profiles showed good agreement with the actual well-log data, exhibiting sharp boundaries between upper and lower layers and demonstrating high resolution. However, the AVA inversion results initialized with the ES-MDA solution showed noticeably higher quality than those obtained using the low-frequency trend model.

In this seismic line, the target layer was located approximately between 2.42 seconds and 2.74 seconds and consisted of interbedded sandstone and mudstone layers of the river deposit. The riverbed sand bodies are stacked vertically and migrate laterally. In the western part of the seismic line, two major faults divide the target layer into three sections. The interfaces between the interbedded sandstone and mudstone layers, and the positions of the fault planes, are crucial indicators for reservoir characterization. As indicated by the arrows in Figures 12–14, the resolution of inverted elastic parameters obtained using AVA inversion with the ES-MDA initial solution improved. In addition, as indicated by the ovals in Figure 12, the inverted V_p matched the well-log curve more accurately. In contrast, for AVA inversion initialized with the low-frequency trend model, the interfaces between the interbedded sandstone and mudstone layers were less distinct, and the fault break points appeared blurred. Overall, AVA inversion using the ES-MDA initial solution was better and can clearly delineate the interfaces between interbedded sandstone and mudstone layers, as well as the locations of the fault break point, compared with AVA inversion using the low-frequency trend models. Based on the ES-MDA results, which were used as the initial solution for AVA inversion, the resolution was higher than that achieved with the conventional low-frequency prior model. Consequently, the resulting AVA inversion exhibited higher quality and better agreement with the actual well-log data. Many detailed features recovered by ES-MDA were incorporated into the AVA inversion results.

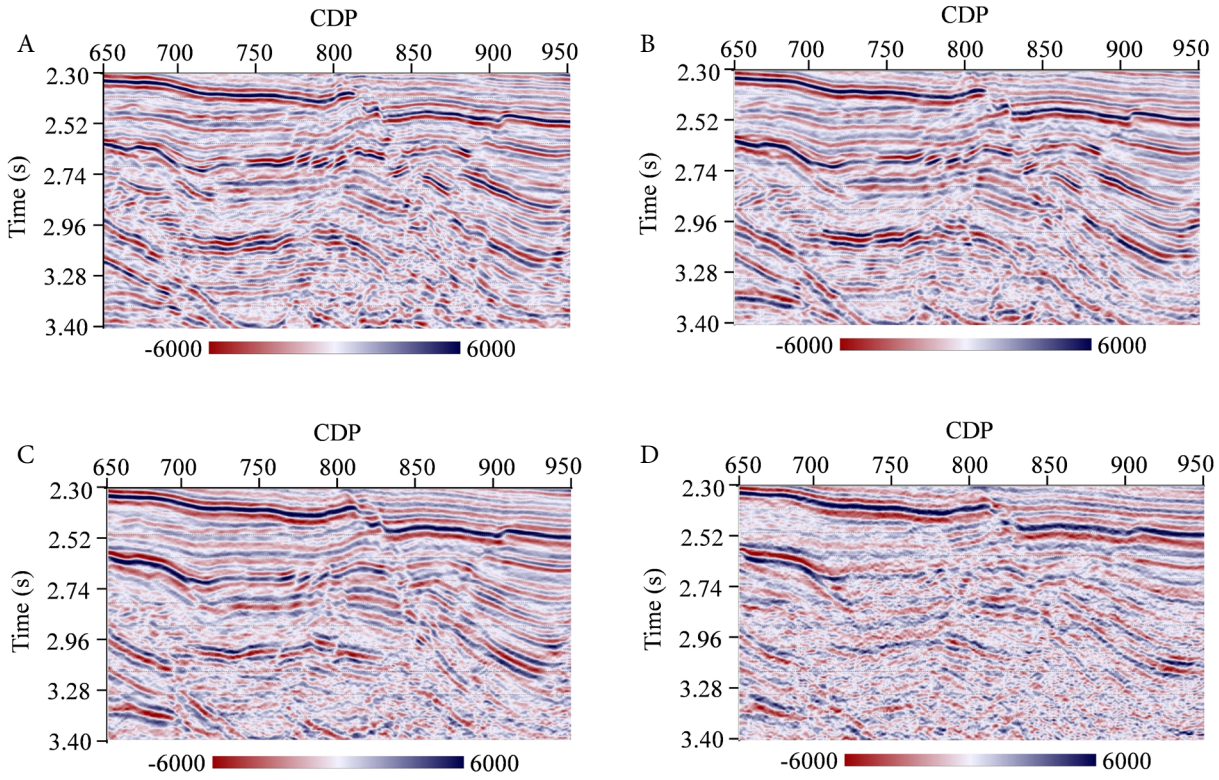

Figure 10. The seismic data sections with four different partial angles. (A) 2–12°; (B) 12–22°; (C) 22–32°; and (D) 32–42°.
Abbreviation: CDP: Common depth point.

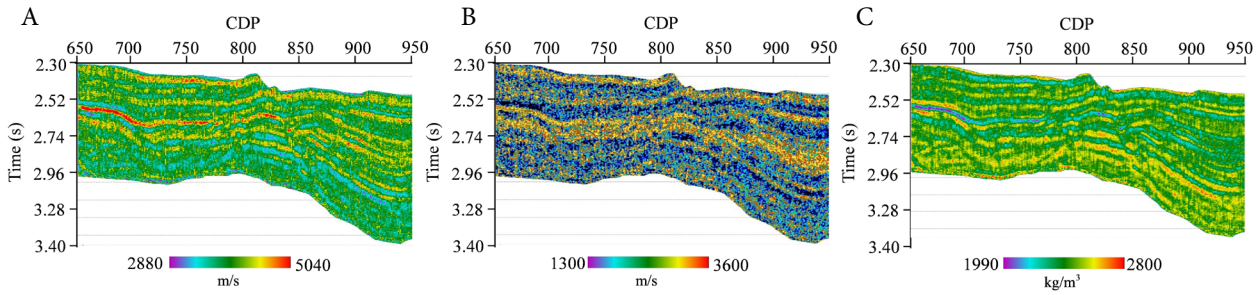

Figure 11. The results of ES-MDA. (A) V_p. (B) V_s. (C) ρ.
Abbreviations: CDP: Common depth point; ES-MDA: Ensemble smoother with multiple data assimilation; ρ: Density; V_p: P-wave velocity; V_s: S-wave velocity.

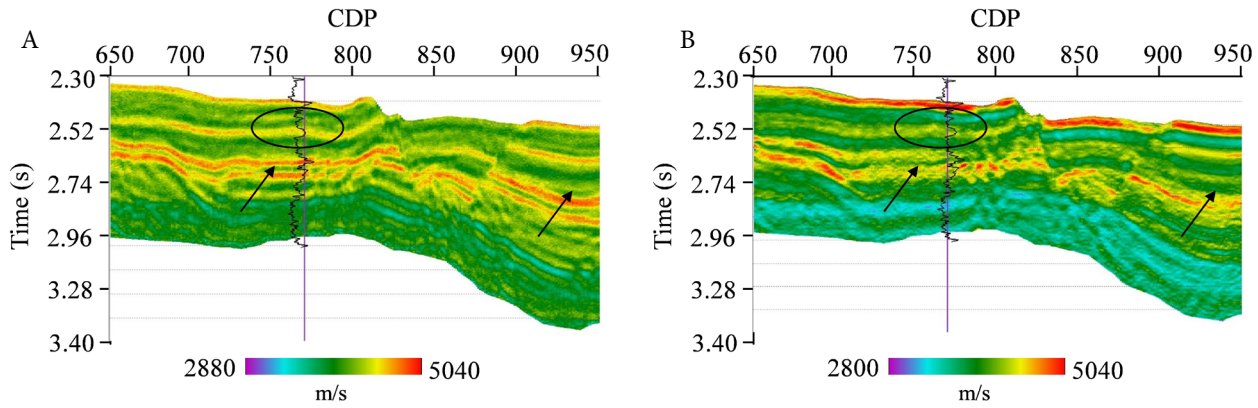

Figure 12. The inverted V_p. (A) AVA inversion with ES-MDA solution. (B) AVA inversion with a low-frequency trend model.
Abbreviations: AVA: Amplitude variation with incident angle inversion; CDP: Common depth point; ES-MDA: Ensemble smoother with multiple data assimilation; V_p: P-wave velocity.

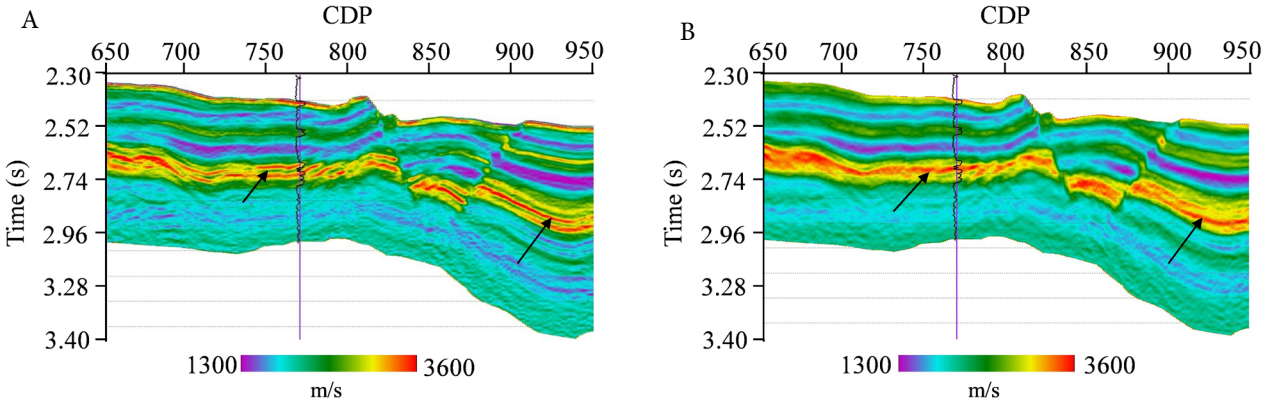

Figure 13. The inverted V_s. (A) AVA inversion with ES-MDA solution. (B) AVA inversion with a low-frequency trend model.
Abbreviations: AVA: Amplitude variation with incident angle inversion; CDP: Common depth point; ES-MDA: Ensemble smoother with multiple data assimilation; V_s: S-wave velocity.

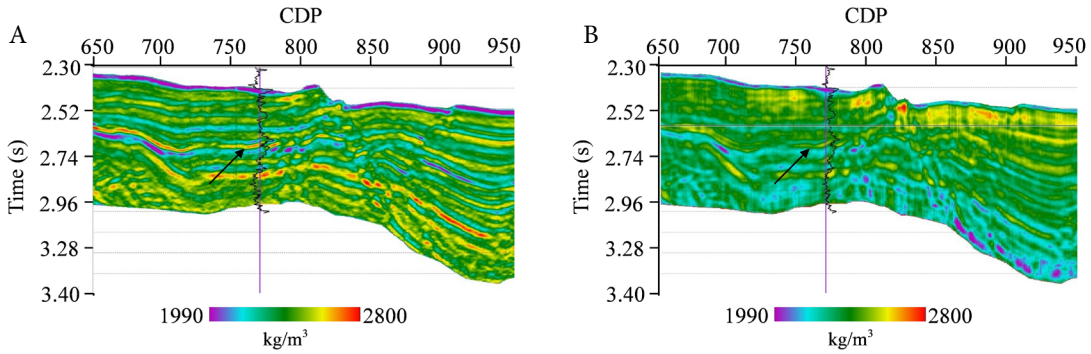

Figure 14. The inverted ρ. (A) AVA inversion with ES-MDA solution. (B) AVA inversion with a low-frequency trend model.
Abbreviations: AVA: Amplitude variation with incident angle inversion; CDP: Common depth point; ES-MDA: Ensemble smoother with multiple data assimilation; ρ: Density.

4. Discussion

In many seismic inversion methods, the objective function is non-linear due to a non-linear forward operator or the regularization term. When gradient-based algorithms are adopted, the choice of the initial model is extremely crucial. If the initial model is far from the optimal solution, the optimization may become trapped in a local minimum, and the inversion methods will yield only sub-optimal solutions. In contrast, stochastic optimal algorithms can often achieve the optimal or near-optimal solution; however, their computational cost becomes prohibitively high when dealing with large-dimensional geophysical data, as is typical in seismic reservoir characterization. Table 2 summarizes the computation times for AVA inversion, ES-MDA inversion, and AVA inversion using ES-MDA results as the initial solution in the numerical model tests. It can be seen that the computation times for AVA with a smooth initial model and AVA with ES-MDA as the initial solution are approximately equivalent. The majority of the computational cost of the proposed method in this paper is devoted to applying ES-MDA. Consequently, the number of high-dimensional ensemble models for the whole 2D profiles or 3D volumes becomes prohibitively large, making direct application to real datasets impractical. Simulating complete 2D profiles or 3D volumes necessitates the consideration of both vertical and lateral constraints. Additionally, this approach requires an extremely large amount of computation, likely exceeding the capabilities of a personal computer, and the real data would be extensive. The novelty of this work lies in combining the strengths of gradient-based algorithms and stochastic optimal algorithms while mitigating their respective limitations. Specifically, ES-MDA was first applied in a computationally feasible, trace-by-trace manner to take advantage of its ability to approximate the optimal solution. The resulting ES-MDA output was then used as a high-quality initial model for IRLS-based AVA inversion. This approach improves the accuracy of AVA inversion due to the high-quality nature of the ES-MDA solution.

In the current ES-MDA implementation, no lateral constraints were applied. Consequently, the lateral continuity of the ES-MDA solution was very poor, which somewhat limited its approximation accuracy. Considering computational efficiency, it would be beneficial to incorporate a degree of lateral constraints when simulating each trace to further improve the ES-MDA accuracy. For example, the similarity of adjacent seismic traces could be considered when drawing samples from the prior distribution of model parameters to form the initial ensemble using stochastic simulation (i.e., the solutions of adjacent seismic traces could serve as the reference for simulating the current trace. This approach could be explored in future work.

Table 2. Computation times of the methods

Methods	Time (s)
AVA with a smooth model as the initial solution	1,611.8830
ES-MDA	27,857
AVA with ES-MDA as the initial solution	1,572.9160

Abbreviations: AVA: Amplitude variation with incident angle inversion; ES-MDA: Ensemble smoother with multiple data assimilation.

5. Conclusion

In AVA inversion, Cauchy sparse regularization is frequently used to constrain the inverse problem and obtain physically meaningful results. The non-linear nature

of Cauchy regularization implies a strong dependence of the inversion quality on the initial model. In complex geological settings, the initial solution must be close to the optimal solution to ensure accurate inversion results. In this study, we successfully developed and validated an AVA inversion method that combines ES-MDA with Cauchy regularization. Specifically, the ES-MDA solution was used as the initial model for AVA inversion with Cauchy regularization. ES-MDA is a stochastic approach that integrates collective thinking with a multi-data assimilation mechanism. Its solution provides a good approximation of the optimal solution, helping to overcome the limitations of AVA inversion related to the choice of initial model.

Both numerical simulations and real-world case studies demonstrated that the proposed method improves the accuracy of estimated elastic parameters compared to AVA inversion with a smooth initial model. The research findings offer new technical approaches for seismic prediction with AVA inversion in complex reservoirs, holding practical application value. Seismic reservoir characterization often involves geophysical data of very high dimensionality, making the number of high-dimensional ensemble models for the full 2D profiles or 3D volumes prohibitively large. To address this, ES-MDA was not applied to the full seismic data profile; instead, it is performed in a computationally feasible, trace-by-trace manner, leveraging its ability to approximate the optimal solution without requiring full–scale high–dimensional simulations.

Acknowledgments

The researchers extend their gratitude to Sinopec Shengli Oil & Gasfield Company for providing the data and technical assistance throughout this study.

Funding

This work was supported by the National Natural Science Foundation of China under grant number: 42204123.

Conflict of interest

The authors declare they have no competing interests.

Author contributions

Conceptualization: Ronghuo Dai
Formal analysis: Rui Liao
Investigation: Rui Liao
Methodology: Ronghuo Dai
Writing–original draft: Rui Liao
Writing–review & editing: Ronghuo Dai

Availability of data

The data that support the findings of this study are available from the corresponding author upon reasonable request.

References

1. Aki K, Richards PG. *Quantitative Seismology: Theory and Methods*. Vols 1-2. San Francisco, CA: Freeman; 1980:160-195.
2. Zoeppritz K, Erdbebenwellen VB. On the reflection and propagation of seismic waves. *Gottinger Nachrichten*. 1919;1:66-84.
3. Shuey R. A simplification of the Zoeppritz equations. *Geophysics*. 1985;50(4):609-614.
   doi: 10.1190/1.1441936
4. Russell BH, Gray D, Hampson DP. Linearized AVO and poroelasticity. *Geophysics*. 2011;76(3):C19-C29.
   doi: 10.1190/1.3555082
5. Xiao S, Ba J, Guo Q, Carcione JM, Zhang L, Luo C. Seismic pre-stack AVA inversion scheme based on lithology constraints. *J Geophys Eng*. 2020;17(3):411-428.
   doi: 10.1093/jge/gxaa001
6. Bao Y, Chen J, Liu XB, Zhao ZC. Joint PP and PS anisotropic AVO inversion using the exact Zoeppritz equations. *J Seism Explor*. 2021;30(6):529-544.
7. Ye T, Li J, Ding W, Long F, Yang J, Liu C. Application of full-angle prestack density inversion for deep tidal-flat thin dolomite reservoirs. *Geophys Prospect Pet*. 2024;63(6):1203-1213. [In Chinese].
   doi: 10.12431/issn.1000-1441.2024.63.06.011
8. Zhou L, Li J, Chen X, Liu X, Chen L. Prestack amplitude versus angle inversion for Young's modulus and Poisson's ratio based on the exact Zoeppritz equations. *Geophys Prospect*. 2017;65(6):1462-1476.
   doi: 10.1111/1365-2478.12493
9. Li H. Prestack seismic prediction technique for ultra-deep carbonate reservoirs in Shunbei field. *Geophys Prospect Pet*. 2025;64(4):736-748. [In Chinese].
   doi: 10.12431/issn.1000-1441.2025.0027
10. Lehocki I, Mukerji T, Avseth P, Jensen EH. Algorithms for extraction of reliable density ratios from pre-stack seismic data—Part 1: Theory. *Geophys Prospect*. 2025;73(6):e70029.
    doi: 10.1111/1365-2478.70029
11. Sun W, Chen Z, Wang R, Duan M. Research on fluid identification technology of submarine fan reservoirs: A case study of Meishan Formation in Ledong–Lingshui Sag. *Geophys Prospect Pet*. 2025;64(6):1107-1117. [In Chinese].
    doi: 10.12431/issn.1000-1441.2024.0230
12. Zhang P, Xiao Y, Xiao P, Chen P, Xu W. A fluid factor inversion method using the frequency-domain two-step

sub-band regularization. *J Seism Explor*. 2025;34(5):1-17.

doi: 10.36922/JSE025310048

13. Sacchi MD. Reweighting strategies in seismic deconvolution. *Geophys J Int*. 1997;129(3):651-656.

doi: 10.1111/j.1365-246X.1997.tb04500.x

14. Alemie W, Sacchi MD. High-resolution three-term AVO inversion by means of a Trivariate Cauchy probability distribution. *Geophysics*. 2011;76(3):R43-R55.

doi: 10.1190/1.3554627

15. Zhang F, Dai R. Nonlinear inversion of pre-stack seismic data using variable metric method. *J Appl Geophys*. 2016;129:111-125.

doi: 10.1016/j.jappgeo.2016.03.035

16. Dai R, Yin C. An iterative re-weighting algorithm for element to solve sparsity-regularized linear inverse problem and an application in sparse-spike deconvolution of seismic data. *IEEE Geosci Remote Sens Lett*. 2025;22:7506605.

doi: 10.1109/LGRS.2025.3574446

17. Zhang R, Castagna J. Seismic sparse-layer reflectivity inversion using basis pursuit decomposition. *Geophysics*. 2011;76(6):R147-R158.

doi: 10.1190/geo2011-0103.1

18. Zong Z, Yin X, Wu G. Geofluid discrimination incorporating poroelasticity and seismic reflection inversion. *Surv Geophys*. 2015;36(5):659-681.

doi: 10.1007/s10712-015-9330-6

19. Wang Y. Basics of seismic inversion. In: *Seismic Inversion: Theory and Applications*. John Wiley & Sons; 2016:45-80.

doi: 10.1002/9781119258032.ch1

20. Emerick AA, Reynolds AC. Ensemble smoother with multiple data assimilation. *Comput Geosci*. 2013;55:3-15.

doi: 10.1016/j.cageo.2012.03.011

21. Gineste M, Eidsvik J. Seismic waveform inversion using the ensemble Kalman smoother. In: Proceedings of the *79th EAGE conference and exhibition 2017*; June 12-15, 2017; Paris, France. European Association of Geoscientists & Engineers; 2017:1-5.

doi: 10.3997/2214-4609.201700794

22. Grana D, Mukerji T, Doyen P. *Seismic Reservoir Modeling: Theory, Examples, and Algorithms*. John Wiley & Sons; 2021:130-145. Available from: https://www.wiley.com/en-us/Seismic+Reservoir+Modeling%3A+Theory%2C+Examples%2C+and+Algorithms-p-9781119086185 [Last accessed in December 2025].

23. Li C, Zhang F. Amplitude-versus-angle inversion based on the l1-norm-based likelihood function and the total variation regularization constraint. *Geophysics*. 2017;82(3):R173-R182.

doi: 10.1190/geo2016-0182.1

24. Dai R, Yang J. Amplitude-versus-angle (AVA) inversion for pre-stack seismic data with L0-Norm-Gradient regularization. *Mathematics*. 2023;11(4):880.

doi: 10.3390/math11040880

25. Fatti JL, Smith GC, Vail PJ, Strauss PJ, Levitt PR. Detection of gas in sandstone reservoirs using AVO analysis: A 3-D seismic case history using the Geostack technique. *Geophysics*. 1994;59(9):1362-1376.

doi: 10.1190/1.1443695